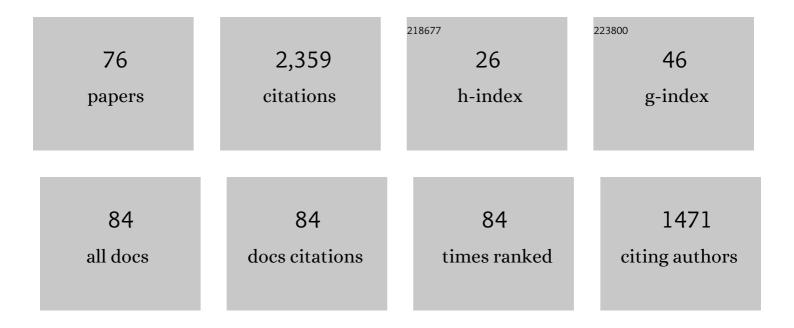
List of Publications by Year in descending order

Source: https://exaly.com/author-pdf/1079508/publications.pdf Version: 2024-02-01



#	Article	IF	CITATIONS
1	Parahydrogenâ€Based Hyperpolarization for Biomedicine. Angewandte Chemie - International Edition, 2018, 57, 11140-11162.	13.8	251
2	PASADENA Hyperpolarization of Succinic Acid for MRI and NMR Spectroscopy. Journal of the American Chemical Society, 2008, 130, 4212-4213.	13.7	170
3	A hyperpolarized equilibrium for magnetic resonance. Nature Communications, 2013, 4, 2946.	12.8	126
4	PASADENA hyperpolarization of 13C biomolecules: equipment design and installation. Magnetic Resonance Materials in Physics, Biology, and Medicine, 2009, 22, 111-121.	2.0	123
5	Toward Biocompatible Nuclear Hyperpolarization Using Signal Amplification by Reversible Exchange: Quantitative <i>in Situ</i> Spectroscopy and High-Field Imaging. Analytical Chemistry, 2014, 86, 1767-1774.	6.5	105
6	A continuousâ€flow, highâ€throughput, highâ€pressure parahydrogen converter for hyperpolarization in a clinical setting. NMR in Biomedicine, 2013, 26, 124-131.	2.8	83
7	Quality assurance of PASADENA hyperpolarization for 13C biomolecules. Magnetic Resonance Materials in Physics, Biology, and Medicine, 2009, 22, 123-134.	2.0	79
8	Dental MRI using wireless intraoral coils. Scientific Reports, 2016, 6, 23301.	3.3	78
9	Dental MRI: Imaging of soft and solid components without ionizing radiation. Journal of Magnetic Resonance Imaging, 2012, 36, 841-846.	3.4	75
10	On the spin order transfer from parahydrogen to another nucleus. Journal of Magnetic Resonance, 2012, 225, 25-35.	2.1	68
11	Quantitative description of the SABRE process: rigorous consideration of spin dynamics and chemical exchange. RSC Advances, 2016, 6, 24470-24477.	3.6	55
12	Parawasserstoffâ€basierte Hyperpolarisierung für die Biomedizin. Angewandte Chemie, 2018, 130, 11310-11333.	2.0	54
13	Instrumentation for Hydrogenative Parahydrogen-Based Hyperpolarization Techniques. Analytical Chemistry, 2022, 94, 479-502.	6.5	52
14	Magnetic resonance imaging of intraoral hard and soft tissues using an intraoral coil and FLASH sequences. European Radiology, 2016, 26, 4616-4623.	4.5	44
15	Continuous Reâ€hyperpolarization of Nuclear Spins Using Parahydrogen: Theory and Experiment. ChemPhysChem, 2014, 15, 2451-2457.	2.1	41
16	Wholeâ€body MRIâ€based fat quantification: A comparison to air displacement plethysmography. Journal of Magnetic Resonance Imaging, 2014, 40, 1437-1444.	3.4	40
17	Molecular MRI in the Earth's Magnetic Field Using Continuous Hyperpolarization of a Biomolecule in Water. Journal of Physical Chemistry B, 2016, 120, 5670-5677.	2.6	37
18	Zero-field nuclear magnetic resonance of chemically exchanging systems. Nature Communications, 2019, 10, 3002.	12.8	36

#	Article	IF	CITATIONS
19	In vivo 13C-MRI using SAMBADENA. PLoS ONE, 2018, 13, e0200141.	2.5	35
20	Simultaneous characterization of tumor cellularity and the Warburg effect with PET, MRI and hyperpolarized ¹³ C-MRSI. Theranostics, 2018, 8, 4765-4780.	10.0	35
21	Parahydrogenâ€Induced Polarization of Amino Acids. Angewandte Chemie - International Edition, 2021, 60, 23496-23507.	13.8	34
22	A battery-driven, low-field NMR unit for thermally and hyperpolarized samples. Magnetic Resonance Materials in Physics, Biology, and Medicine, 2013, 26, 491-499.	2.0	33
23	Chemical Exchange Reaction Effect on Polarization Transfer Efficiency in SLIC-SABRE. Journal of Physical Chemistry A, 2018, 122, 9107-9114.	2.5	33
24	¹⁵ N MRI of SLICâ€SABRE Hyperpolarized ¹⁵ N‣abelled Pyridine and Nicotinamide. Chemistry - A European Journal, 2019, 25, 8465-8470.	3.3	33
25	Virtual implant planning and fully guided implant surgery using magnetic resonance imaging—Proof of principle. Clinical Oral Implants Research, 2020, 31, 575-583.	4.5	29
26	Pulse-Programmable Magnetic Field Sweeping of Parahydrogen-Induced Polarization by Side Arm Hydrogenation. Analytical Chemistry, 2020, 92, 1340-1345.	6.5	28
27	MR Spectroscopy in Diagnosis and Neurological Decision-Making. Seminars in Neurology, 2008, 28, 407-422.	1.4	27
28	Fast volumetric spatial-spectral MR imaging of hyperpolarized 13C-labeled compounds using multiple echo 3D bSSFP. Magnetic Resonance Imaging, 2010, 28, 459-465.	1.8	27
29	SAMBADENA Hyperpolarization of ¹³ Câ€Succinate in an MRI: Singletâ€Triplet Mixing Causes Polarization Loss. ChemistryOpen, 2019, 8, 728-736.	1.9	25
30	Simulating Nonâ€linear Chemical and Physical (CAP) Dynamics of Signal Amplification By Reversible Exchange (SABRE). Chemistry - A European Journal, 2019, 25, 7659-7668.	3.3	25
31	Continuous Radio Amplification by Stimulated Emission of Radiation using Parahydrogen Induced Polarization (PHIPâ€RASER) at 14 Tesla. ChemPhysChem, 2020, 21, 667-672.	2.1	25
32	Open-source, partially 3D-printed, high-pressure (50-bar) liquid-nitrogen-cooled parahydrogen generator. Magnetic Resonance, 2021, 2, 49-62.	1.9	22
33	Magnetic resonance imaging—a diagnostic tool for postoperative evaluation of dental implants: a case report. Oral Surgery, Oral Medicine, Oral Pathology and Oral Radiology, 2018, 125, e103-e107.	0.4	21
34	Molecular Imaging of Activated Platelets Allows the Detection of Pulmonary Embolism with Magnetic Resonance Imaging. Scientific Reports, 2016, 6, 25044.	3.3	18
35	Metabolic and Molecular Imaging with Hyperpolarised Tracers. Molecular Imaging and Biology, 2018, 20, 902-918.	2.6	18
36	Parahydrogen-Induced Polarization Relayed via Proton Exchange. Journal of the American Chemical Society, 2021, 143, 13694-13700.	13.7	18

#	Article	IF	CITATIONS
37	A mild case of molybdenum cofactor deficiency defines an alternative route of MOCS1 protein maturation. Journal of Inherited Metabolic Disease, 2018, 41, 187-196.	3.6	16
38	Non-contrast-enhanced magnetic resonance imaging for visualization and quantification of endovascular aortic prosthesis, their endoleaks and aneurysm sacs at 1.5†T. Magnetic Resonance Imaging, 2019, 60, 164-172.	1.8	16
39	Dynamic 2D and 3D mapping of hyperpolarized pyruvate to lactate conversion in vivo with efficient multiâ€echo balanced steadyâ€state free precession at 3 T. NMR in Biomedicine, 2020, 33, e4291.	2.8	16
40	<scp>Pseudoâ€Enhancement</scp> in Intracranial Aneurysms on <scp>Blackâ€Blood MRI</scp> : Effects of Flow Rate, Spatial Resolution, and Additional Flow Suppression. Journal of Magnetic Resonance Imaging, 2021, 54, 888-901.	3.4	16
41	Selective excitation of hydrogen doubles the yield and improves the robustness of parahydrogen-induced polarization of low-γ nuclei. Physical Chemistry Chemical Physics, 2021, 23, 26645-26652.	2.8	15
42	Quasi-continuous production of highly hyperpolarized carbon-13 contrast agents every 15 seconds within an MRI system. Communications Chemistry, 2022, 5, .	4.5	15
43	Performance and reproducibility of 13C and 15N hyperpolarization using a cryogen-free DNP polarizer. Scientific Reports, 2022, 12, .	3.3	15
44	Multiple Quantum Coherences Hyperpolarized at Ultra‣ow Fields. ChemPhysChem, 2019, 20, 2823-2829.	2.1	14
45	3Dâ€printed, patientâ€specific intracranial aneurysm models: From clinical data to flow experiments with endovascular devices. Medical Physics, 2021, 48, 1469-1484.	3.0	14
46	Coherent Evolution of Signal Amplification by Reversible Exchange in Two Alternating Fields (alt‧ABRE). ChemPhysChem, 2021, 22, 2381-2386.	2.1	14
47	Dynamic <i>in vivo</i> monitoring of fracture healing process in response to magnesium implant with multimodal imaging: pilot longitudinal study in a rat external fixation model. Biomaterials Science, 2022, 10, 1532-1543.	5.4	14
48	Only Para-Hydrogen Spectroscopy (OPSY) Revisited: In-Phase Spectra for Chemical Analysis and Imaging. Journal of Physical Chemistry A, 2018, 122, 8948-8956.	2.5	13
49	Intratumoral Distribution of Lactate and the Monocarboxylate Transporters 1 and 4 in Human Glioblastoma Multiforme and Their Relationships to Tumor Progression-Associated Markers. International Journal of Molecular Sciences, 2020, 21, 6254.	4.1	13
50	Telmisartan prevents high-fat diet-induced neurovascular impairments and reduces anxiety-like behavior. Journal of Cerebral Blood Flow and Metabolism, 2021, 41, 2356-2369.	4.3	13
51	Dendronised Ni(<scp>ii</scp>) porphyrins as photoswitchable contrast agents for MRI. Physical Chemistry Chemical Physics, 2019, 21, 24296-24299.	2.8	12
52	High-Resolution Single Tooth MRI With an Inductively Coupled Intraoral Coil—Can MRI Compete With CBCT?. Investigative Radiology, 2022, 57, 720-727.	6.2	11
53	Whole-Brain <i>N</i> -Acetylaspartate MR Spectroscopic Quantification: Performance Comparison of Metabolite versus Lipid Nulling. American Journal of Neuroradiology, 2008, 29, 1441-1445.	2.4	10
54	Multimodal Targeted Nanoparticle-Based Delivery System for Pancreatic Tumor Imaging in Cellular and Animal Models. Current Pharmaceutical Design, 2022, 28, 313-323.	1.9	10

#	Article	IF	CITATIONS
55	Frequencyâ€Selective Manipulations of Spins allow Effective and Robust Transfer of Spin Order from Parahydrogen to Heteronuclei in Weaklyâ€Coupled Spin Systems. ChemPhysChem, 2022, 23, .	2.1	10
56	Selective excitation doubles the transfer of parahydrogen-induced polarization to heteronuclei. Physical Chemistry Chemical Physics, 2021, 23, 14146-14150.	2.8	9
57	Modular Coils with Low Hydrogen Content Especially for MRI of Dry Solids. PLoS ONE, 2015, 10, e0139763.	2.5	9
58	OnlyParahydrogen SpectrosopY (OPSY) pulse sequences – One does not fit all. Journal of Magnetic Resonance, 2018, 297, 86-95.	2.1	8
59	Lifetime of Para hydrogen in Aqueous Solutions and Human Blood. ChemPhysChem, 2019, 20, 2408-2412.	2.1	8
60	Optimization of 3D phase contrast venography for the assessment of the cranio-cervical venous system at 1.5ÂT. Neuroradiology, 2019, 61, 293-304.	2.2	8
61	High field <i>para</i> hydrogen induced polarization of succinate and phospholactate. Physical Chemistry Chemical Physics, 2021, 23, 2320-2330.	2.8	8
62	Ni(II)porphyrins as pH dependent light-driven coordination-induced spin-state switches (LD-CISSS) in aqueous solution. Journal of Porphyrins and Phthalocyanines, 2020, 24, 480-488.	0.8	7
63	In vitro singlet state and zero-quantum encoded magnetic resonance spectroscopy: Illustration with N-acetyl-aspartate. PLoS ONE, 2020, 15, e0239982.	2.5	6
64	Symmetry Constraints on Spin Order Transfer in Parahydrogen-Induced Polarization (PHIP). Symmetry, 2022, 14, 530.	2.2	6
65	Evaluation of BP-ONJ in osteopenic and healthy sheep: comparing ZTE-MRI with µCT. Dentomaxillofacial Radiology, 2016, 45, 20150250.	2.7	4
66	Coherent polarization transfer in chemically exchanging systems. Physical Chemistry Chemical Physics, 2020, 22, 8963-8972.	2.8	4
67	Catalytic Hydrogenation of Trivinyl Orthoacetate: Mechanisms Elucidated by Parahydrogen Induced Polarization. ChemPhysChem, 2021, 22, 370-377.	2.1	4
68	Influence of Spatial Resolution and Compressed SENSE Acceleration Factor on Flow Quantification with 4D Flow MRI at 3 Tesla. Tomography, 2022, 8, 457-478.	1.8	4
69	A realistic way to investigate the design, and mechanical properties of flow diverter stents. Expert Review of Medical Devices, 2021, 18, 569-579.	2.8	3
70	MRI. , 2017, , 227-324.		2
71	Simulating Nonâ€linear Chemical and Physical (CAP) Dynamics of Signal Amplification By Reversible Exchange (SABRE). Chemistry - A European Journal, 2019, 25, 7580-7580.	3.3	2
72	Thinâ€Film Patient‧pecific Flow Diverter Stents for the Treatment of Intracranial Aneurysms. Advanced Materials Technologies, 2021, 6, 2100384.	5.8	2

#	Article	IF	CITATIONS
73	Parawasserstoffâ€induzierte Polarisation von Aminosären. Angewandte Chemie, 2021, 133, 23688.	2.0	2
74	Luminal enhancement in intracranial aneurysms: fact or feature?—A quantitative multimodal flow analysis. International Journal of Computer Assisted Radiology and Surgery, 2021, 16, 1999-2008.	2.8	2
75	NMR Spectroscopy Techniques: Hyperpolarization for Sensitivity Enhancement. , 2018, , 168-168.		1
76	Response to the letter to the editor regarding "Magnetic resonance imaging (MRI)—a diagnostic tool for postoperative evaluation of dental implants: a case report― Oral Surgery, Oral Medicine, Oral Pathology and Oral Radiology, 2018, 126, 444-445.	0.4	0